Available online at www.sciencedirect.com

SciVerse ScienceDirect

Ceramics International 38 (2012) 2551–2562

CERAMICS INTERNATIONAL

www.elsevier.com/locate/ceramint

Dc field induced optical effects in ZnF_2–PbO–TeO_2:TiO_2 glass ceramics

N. Narasimha Rao [a], I.V. Kityk [b], V. Ravi Kumar [a,*], Ch. Srinivasa Rao [a], M. Piasecki [c], P. Bragiel [c], N. Veeraiah [a]

[a] Department of Physics, Acharya Nagarjuna University – Nuzvid Campus, Nuzvid 521 201, AP, India
[b] Electrical Engineering Department, Technical University of Czestochowa, Aleja Armii, Krajowej 17/19, PL-42-201 Czestochowa, Poland
[c] Institute of Physics, J. Dluygosz University, Armii Krajowej 13.15, Czestochowa, Poland

Received 2 September 2011; accepted 9 November 2011
Available online 18 November 2011

Abstract

ZnF_2–PbO–TeO_2 glasses doped with different concentrations of TiO_2 were synthesized and subsequently crystallized. The prepared samples were characterized by XRD, SEM and DSC. IR, ESR and optical absorption were studied to explore the influence of titanium valance states and their coordination with oxygen on structural and optoelectronic aspects of the samples. These studies have indicated that there is a possibility for the titanium ions to exist in Ti^{3+} and Ti^{4+} states in these glass ceramics and participate in the glass network forming. Finally, we have undertaken second harmonic generation (after the samples were dc field treated at elevated temperatures) with 10 ns Er^{3+}: glass laser (of wavelength 1540 nm with power densities up to 1.5 GW/cm^2) and birefringence studies (in the wavelength range 420–750 nm) to examine the suitability of these materials for optically operated devices. The results of non linear optical studies were discussed in the light of nature of different micro/nano crystallites ingrained in the glass ceramic samples.

Keywords: B. Spectroscopy; C. Optical properties; D. Glass ceramics

1. Introduction

TeO_2 based glasses are well known due to their high density, high refractive index and high transparency in the far infrared region. Photoinduced study on these glasses has been the subject of high interest in recent years due to their potential applications such as IR domes, optical fibers, modulators, memory devices, optical fiber triggers and laser windows. The understanding of the origin of optical susceptibilities in titled glasses and the corresponding glass ceramics stimulated by ultra-short laser pulses has gained momentum in the recent years. Such studies in fact help in examining the suitability of the materials for potential applications like three-dimensional photonic devices for integrated optics and other laser-operated devices (such as ultrafast optical switches, optical fiber modulators, power limiters, and broad band optical amplifiers) [1,2].

Transparent polar glass ceramics comprising nano/micro-crystallites that are capable of exhibiting piezo-, pyro-, ferroelectric, and nonlinear optical (NLO) properties have been in increasing demand and recognized to be potential multifunctional materials.

Recently, transparent crystallized glasses (composites of crystalline and glassy phases), consisting of nonlinear optical or ferroelectric crystals have received much attention and there have been many reports on the fabrication and characterization of such transparent crystallized glasses [3]. Transparency of glass-ceramics can be retained by controlling the crystallization of a glass precursor with appropriate chemical compositions and appropriate nucleating agent. The general conditions for retention of transparency of glass even after the crystallization include small refractive index difference between the crystalline and residual glass phases, a small birefringence of the crystallites and smaller wavelength of the incident light when compared with that of size of crystallites. Investigations along these lines have been carried out on several glass systems including some silicate, fluoride or oxyfluoride matrices, polymers and thin films [4–8].

* Corresponding author. Tel.: +91 8656 235551; fax: +91 8656 235551.
E-mail address: vrksurya@rediffmail.com (V. Ravi Kumar).

0272-8842/$36.00
doi:10.1016/j.ceramint.2011.11.026

Among a variety of polar glass ceramics that were investigated for various physical properties, tellurium dioxide (TeO_2)-based glasses were promising for use in optically operated devices because of their refractive-index compatibility with those of well-known ferroelectric compounds [9]. Further it has been widely accepted that tellurite glasses are promising nonlinear optical materials for their high third-order optical nonlinear (TONL) susceptibility $\chi^{(3)}$ [10].

The characteristics of glass ceramic depend on the kind and quantity of the crystalline phase formed as well as on the residual glass composition. Hence, the selection of a suitable nucleating agent in the correct concentration and determination of the temperature and the time of nucleation and growth are important factors, in the design of desirable glass ceramic. Among various crystallizing agents, TiO_2 is expected to be more effective mineralizer especially in the glass systems like tellurite exhibiting high optical susceptibilities. Normally, the ions of titanium, exist in the glass in Ti^{4+} state and participate in the glass network forming with different principal polyhedral: TiO_4, TiO_6 and some times with TiO_5 (comprising of trigonal bipyramids) structural units [11,12]. However, there are reports suggesting that these ions may also exist in Ti^{3+} valence state in some of the glass matrices [13,14]. Further the inclusion of Ti^{4+} ions into the tellurite glass ceramic network is substantial advantage to use these materials for optically operated devices, since the empty or unfilled 3d-shells of Ti ions contribute more strongly to the non-linear polarizabilities that can be determined prevailingly by optical/electrical Kerr effect. In Ref. [15], it was found that partial crystallization of the glass-like materials leads to substantial enhancement of the photo-induced SHG. Recently, our group has also reported the second-order non-linear optical effects of antimony borate glasses crystallized with CoO as nucleating agents [16]. From these studies, the optimal concentrations of the dopant ions/crystallizing agents for getting the maximum optically induced effects have been identified.

In the present investigation we explored ZnF_2–PbO–TeO_2 glasses, crystallized them with different concentrations of TiO_2 as nucleating agent and characterized them by variety of techniques (XRD, SEM and DSC) and studied second order susceptibility studies (after the samples were dc field poled at elevated temperatures), photo-induced changes (variations in the refractive index with the probe wavelength) and discussed the correlation between glass structure and non-linear optical (NLO) susceptibilities.

2. Experimental

The detailed compositions of the glasses used in the present study are as follows:

TC_0: $30ZnF_2-10.0PbO-60TeO_2$

TC_5: $30ZnF_2-9.50PbO-60TeO_2$: $0.5TiO_2$

TC_7: $30ZnF_2-9.30PbO-60TeO_2$: $0.7TiO_2$

TC_{10}: $30ZnF_2-9.00PbO-60TeO_2$: $1.0TiO_2$

TC_{15}: $30ZnF_2-8.50PbO-60TeO_2$: $1.5TiO_2$

TC_{20}: $30ZnF_2-8.00PbO-60TeO_2$: $2.0TiO_2$

Analytical grade reagents of ZnF_2, PbO, TeO_2 and TiO_2 powders in appropriate amounts (all in wt%) were thoroughly mixed in an agate mortar and melted in a platinum crucible in the temperature range of 923–1023 K in an automatic temperature controlled furnace for about 30 min. The resultant bubble free melt was then poured in a brass mould and subsequently annealed at 473 K. For the crystallization, the glass specimens were first heated up to crystallization temperature 750–800 K (identified from DSC traces) at the rate of 3 K/min and then were held at the specified temperature for 72 h; samples were cooled slowly (for about 3 h) to the off-set temperature of the crystallization peak (to avoid cracks, voids due to subsequent sudden cooling) and then chilled in air to room temperature.

The samples prepared were mechanically ground and polished to a mirror finish with cerium oxide powder. The final dimensions of the samples used for the measurements are about 1 cm × 1 cm × 0.2 cm. Scanning electron microscopy studies were carried out on these samples to observe the crystallinity using HITACHI S-3400N Scanning Electron Microscope. The crystalline phases in the heat treated samples were identified using Rigaku D/Max ULTIMA III X-ray diffractometer with CuK_α radiation. Differential thermal analysis was carried out by Netzsch Simultaneous DSC/TG Thermal Analyzer STA409C with 32-bit controller to determine the glass transition temperature and crystalline peaks. High temperature furnace together with a sample carrier suitable for C_p measurements and Al_2O_3 crucibles were used. Apparatus was calibrated both for temperature and for sensitivity with melting temperatures and melting enthalpies of the pure metals: Ga, In, Sn, Zn, Al, Ag, Au. All the recordings were carried out in argon (5 N) atmosphere to prevent samples from oxidation. Heating rate was 10 K/min within temperature range 300–1600 K. The density of the glasses was determined with precision up to (±0.0001) by the standard principle of Archimedes' using o-xylene (99.99% pure) as the buoyant liquid. The mass of the samples was measured with an accuracy of 0.1 mg using Ohaus digital balance Model AR2140 for evaluating the density. The refractive index (n) of the samples was measured at $\lambda = 589.3$ nm using Abbe refractometer with monobromo naphthalene as the contact layer between the glass and the refractometer prism to an accuracy of 0.001. Infrared transmission spectra were recorded on a JASCO-FT/IR-5300 spectrophotometer with spectral resolution of 0.1 cm^{-1} in the spectral range 400–2000 cm^{-1} using potassium bromide pellets (300 mg) containing pulverized sample (1.5 mg). These pellets were pressed in a vacuum die at ~680 MPa. The ESR spectra of the fine powders of the samples were recorded at room temperature on E11Z Varian X-band ($\nu = 9.5$ GHz) ESR spectrometer. The optical absorption spectra of the glasses were recorded to a resolution of 0.1 nm at room temperature in

the spectral wavelength range covering 300–1000 nm using JASCO Model V-670 UV–vis–NIR spectrophotometer.

The method of measuring of second order optical susceptibility consists of recording the power of the output spectrally separated second-harmonic wave generated (SHG) intensity for the dc-poled sample as a function of applied electrostatic field at elevated temperatures. The beam of 10 ns pulsed Er^{3+} glass laser with wavelength 1540 nm was focused onto the poled region of the sample up to diameter up to 1–2 mm. The non linear optical effects (controlled by the output SHG signal) were recorded after the achievement of maximal sample's polarization which corresponds to the applied electrostatic strength 4 kV/cm with simultaneous sample's heating up to 400 °C. The incident beam of the 10 ns Er^{3+}: glass laser (of wavelength 1540 nm with power densities varying successively up to 1.5 GW/cm^2 per pulse and frequency repetition about 10 Hz) was used as fundamental laser beam. After 3–4 min of such treatment the dc-induced signal of the SHG started procuring intensity and got saturated within several minutes and finally the output SHG value was recorded. As a reference samples we have used crystals of BiB_3O_6 with the known values of second order susceptibilities. The details of the apparatus used for measuring the SHG are given in Fig. 1.

The study of the dispersion of the induced nonlinearity of the samples was carried out with dc field treatment and with simultaneous registration of the Δn by Senarmont method as described in the Ref. [6]. For this purpose a probe beam possessing varying wavelength (emitted from tungsten–halogen lamp and spectrally separated by spectrophotometer Specord 80M) is allowed to incident upon the sample after polarization by a polarizer. The effective phase retardation due to electrically induced effect of the out coming beam is changed by the quarter wave-plate and the analyzer with nonius regite the angle corresponding to the minimum light transmission by the photo-detector. The set-up allows measuring the birefringence with accuracy up to 10^{-5}. The saturation of the birefringence was achieved after 3–5 min. of treatment by dc field at 4 kV/cm and fixed temperature 400 °C. It should be emphasized here that no macroscopic crack formation could be visualized in these samples after this treatment. The wavelength of the probe beam was varied from 450 to 720 nm. Further details of this technique is described in Ref. [17].

3. Results

From the measured values of the density and average molecular weight M of the samples, various other physical parameters such as titanium ion concentration N_i, mean titanium ion separation R_i, polaron radius R_p in ZnF_2–PbO–TeO_2:TiO_2 glass ceramic samples are evaluated and presented in Table 1. The density of the samples is observed to decrease slightly with the concentration of TiO_2. However due to the crystallization a slight increment in the density compared to that of corresponding amorphous samples is observed.

The scanning microscopy pictures of some of the crystallized samples are shown in Fig. 2. The pictures clearly indicate that the samples contain well defined, randomly distributed crystals of different sizes (varying from 100 to 500 nm) ingrained in glassy matrix. The residual glass phase is acting as interconnecting zones among the crystallized areas, making the samples free of voids and cracks. The pictures further indicate a gradual increase in the volume fraction of crystallites in the samples with increasing concentration of TiO_2. Thus, from these pictures it can also be concluded that TiO_2, enhanced the phase separation tendency of various crystalline phases. The SEM pictures of pre-heated samples exhibited virtually no crystallinity. For the sake of comparison the SEM picture of one of the pre-heated samples is also presented in Fig. 2.

X-ray diffraction patterns for the ZnF_2–PbO–TeO_2 glass ceramic doped with 1.0 wt% of TiO_2 is shown in Fig. 3(a). The patterns exhibited peaks due to variety of crystal phases; some of them are $Pb_5Ti_3F_{19}$, $PbTiO_3$, $PbTi_2O_6$, $PbTeO_3$, Pb_3TeO_5,and $TiTe_3O_8$; the details JCPDS card numbers for these crystalline phases can be found in Ref. [18]. The XRD patterns for all the crystallized glasses are shown in Fig. 3(b). Most interestingly we have observed diffraction peak with significant intensity and full width at half maximum due to $Pb_5Ti_3F_{19}$ crystal phase at about $2\theta = 25.00°$, $27.84°$ and $29.65°$. The presence of such phase clearly suggests that a fraction of the titanium ions exists in Ti^{3+} valence state. However, as the concentration of TiO_2 increased, the intensity of these peaks is found to increase up to 1.0 wt% and then a slight decreasing trend is observed. Another interesting feature of XRD pattern is, presence of clear diffraction peaks at $2\theta = 22.77°$ and $31.97°$ corresponding to $PbTiO_3$ orthorhombic crystal phases; this observation points out that the titanium ions do exist in Ti^{4+} state and participate as

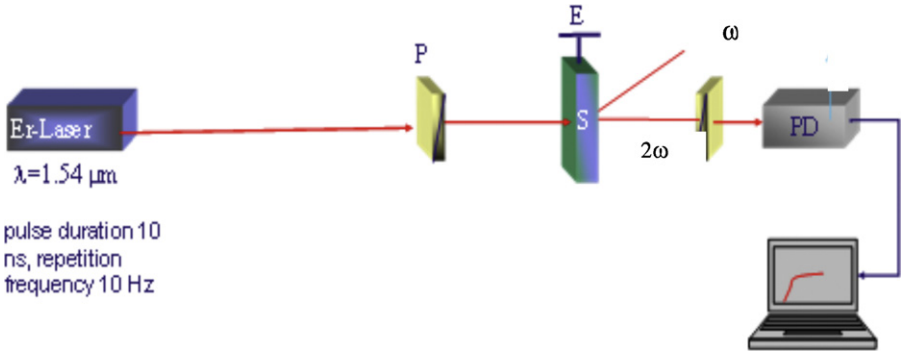

Fig. 1. Principal set-up used for second harmonic generation measurement.

Table 1
Physical parameters of ZnF_2–PbO–TeO_2:TiO_2 glass ceramic samples.

Sample	Density (g/cm^3)	Dopant ion conc. (N_i) ($\times 10^{20}$ ions/cm^3)	Inter ionic distance (Å	Polaron radius (Å)	Refractive index
TC_0	5.660 (5.565)				1.662
TC_5	5.617 (5.506)	1.14	20.62	8.309	1.655
TC_7	5.517 (5.499)	1.57	18.53	7.468	1.653
TC_{10}	5.499 (5.496)	2.24	16.46	6.632	1.649
TC_{15}	5.486 (5.476)	3.55	14.12	5.689	1.642
TC_{20}	5.467 (5.405)	4.51	13.04	5.256	1.633

Density values given in the parenthesis are those of corresponding amorphous samples.

a network former in the glass network. It may be noted here that the XRD pattern of pre-heated samples have not exhibited any sharp peaks (Fig. 3(b)).

In Fig. 4(a) differential scanning calorimetric (DSC) scans for ZnF_2–PbO–TeO_2:TiO_2 glass-ceramics in the temperature region 300–1000 K are presented. For the crystallized glasses, a weak endothermic affect (due to glass transition) in the temperature range 590–610 K is observed. At about 770 K, the DSC thermograms of each glass ceramic samples exhibited well-defined exothermic effects with multiple steps of crystallization temperatures; the auxiliary peaks appear to be weak and spread over a region of approximately 50 K. The variation of enthalpy associated with the primary crystallization peak with the concentration of crystallizing agent is shown as the inset of Fig. 4(a); the enthalpy is observed to decrease with the concentration of crystallizing agent TiO_2. It may be noted here that no multiple steps of crystallization are observed in the thermograms of pre-crystallized samples. To observe the mass change effects during heating process, we have also recorded thermal gravimetric traces for all the samples; in Fig. 4(b), TG traces for two of the samples along with corresponding DSC traces are shown. The analysis up to 1600 K exhibits virtually no change in the mass of the samples.

Fig. 5(a) presents optical absorption spectra of ZnF_2–PbO–TeO_2:TiO_2 glass ceramic samples recorded at room temperature in the wavelength region 300–900 nm. The absorption edge observed at 397 nm for the glass ceramic sample TC_{10} exhibited blue spectral shift with further increase of the concentration of TiO_2. Additionally, the spectrum of all the samples exhibited two clearly resolved absorption bands in the spectral range 550–560 and 660–680 nm. As the concentration of TiO_2 is continued to increase up to 1.0 wt% the half width and intensity of these two bands are observed to increase with a slight shift in the peak positions towards higher wavelength. The summary of the data on optical absorption spectra of these glasses is furnished in Table 2.

From the observed absorption edges, we have evaluated the optical band gaps (E_o) of these samples by drawing Tauc plots [19] (Fig. 5(b)) between $(\alpha\hbar\omega)^{1/2}$ and $\hbar\omega$ as per the equation.

$$\alpha(\omega)\hbar\omega = c(\hbar\omega - E_o)^2 \quad (1)$$

From the extrapolation of the linear portion of the curves of Fig. 5(b), the values of optical band gap (E_o) are determined and are presented in Table 2; the value of E_o with the concentration of TiO_2 exhibited a minimal effect at about 1.0 wt% of TiO_2 (inset of Fig. 5(b)).

ESR spectra for one of the ZnF_2–PbO–TeO_2:TiO_2 glass ceramic samples (TC_{10}) recorded at room temperature is shown in Fig. 6. The spectrum consists of an intense asymmetric spectral line centered at about $g = 1.9485$. The pattern of all other samples exhibited similar behaviour, the half width and

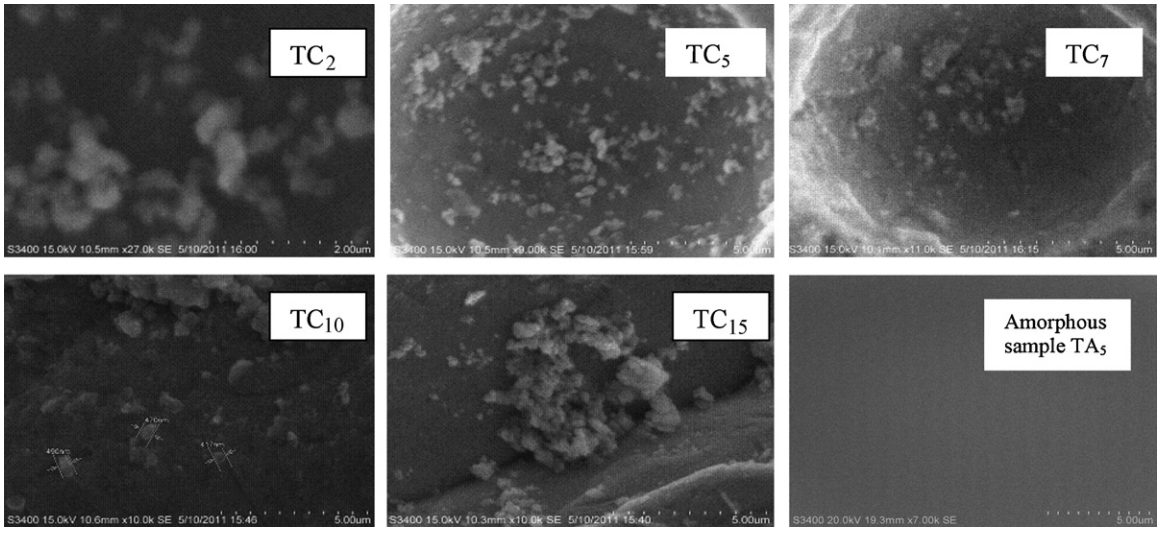

Fig. 2. ZnF_2–PbO–TeO_2 glasses heat treated with different concentrations of TiO_2.

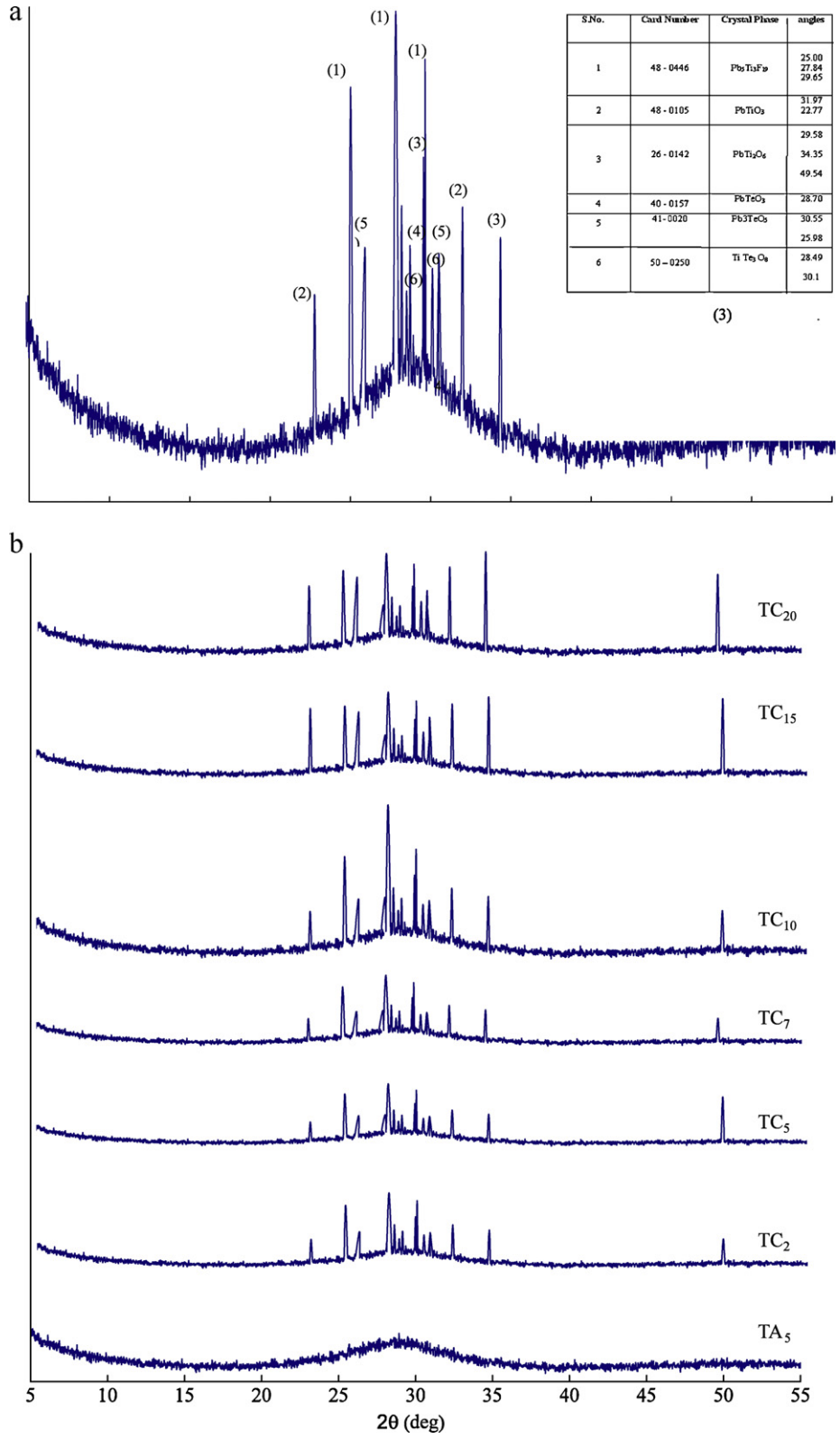

Fig. 3. (a) XRD pattern of ZnF_2–PbO–TeO_2 glass ceramics doped with 1.0 wt% of TiO_2 showing different possible crystal phases. (b) XRD pattern of ZnF_2–PbO–TeO_2 glass ceramics doped with different concentrations of TiO_2. For the sake of comparison, the XRD pattern of one of the pre-crystallized samples (TA_5) is also included.

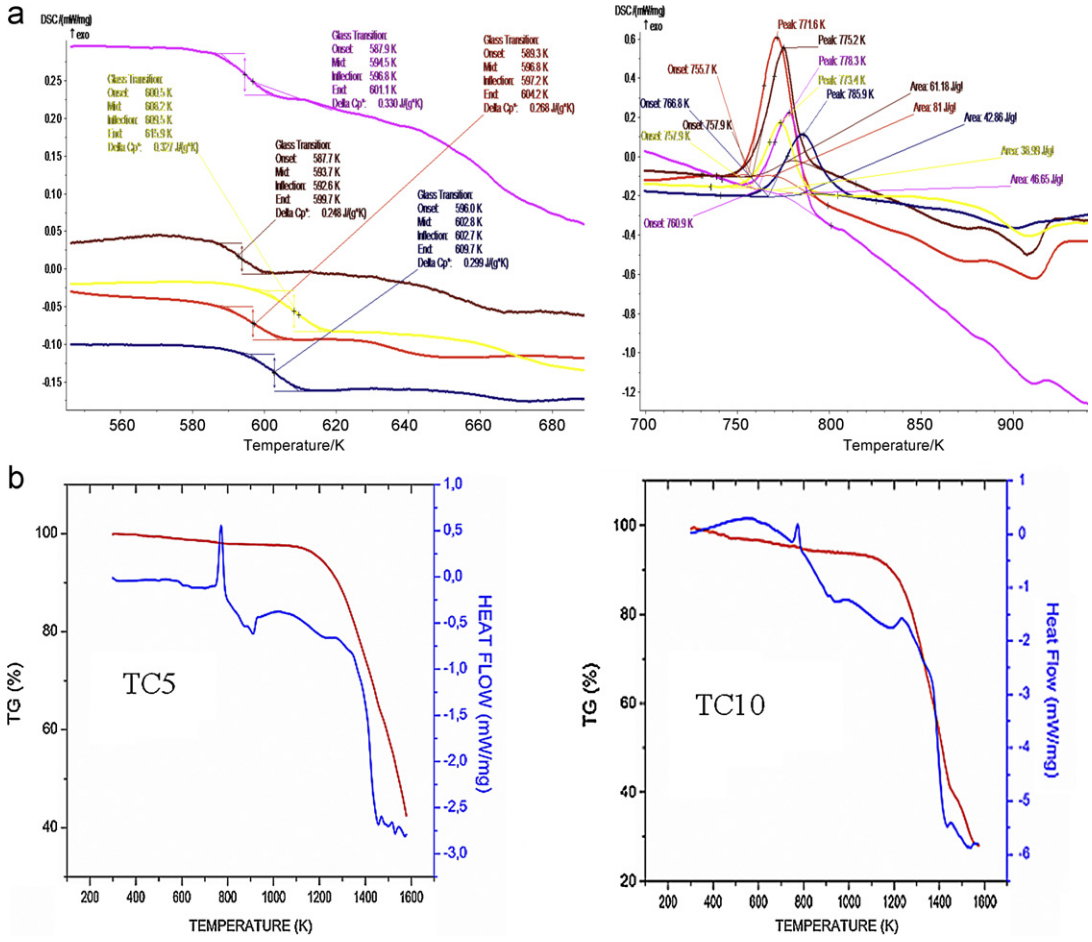

Fig. 4. (a) DSC traces of ZnF_2–PbO–TeO_2 glass ceramics doped with different concentrations of TiO_2. (b) TG traces of ZnF_2–PbO–TeO_2:TiO_2 glass ceramics along with corresponding DSC traces.

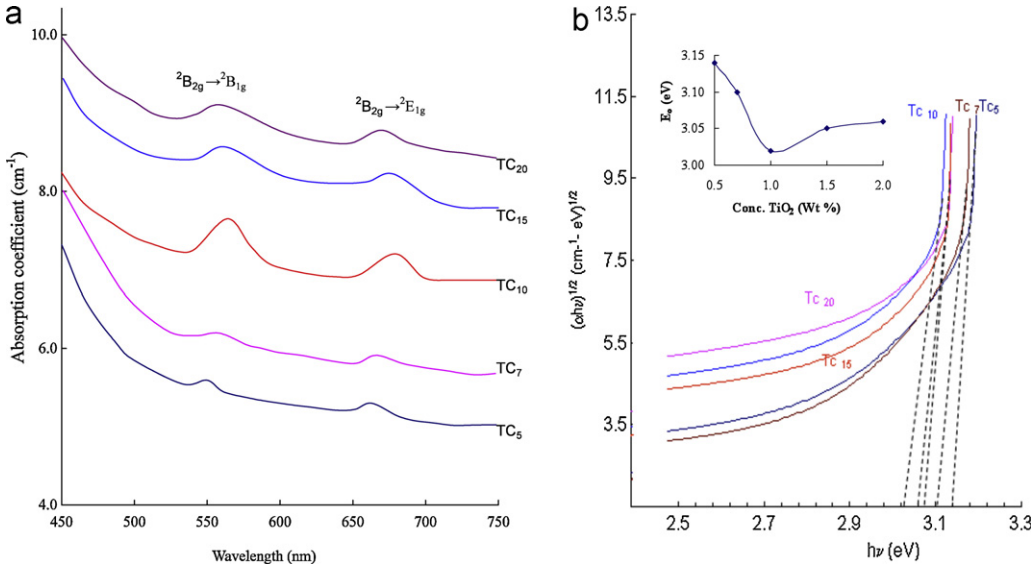

Fig. 5. (a) Optical absorption spectra of ZnF_2–PbO–TeO_2 glasses crystallized with different concentrations of TiO_2. (b) Tauc plots of ZnF_2–PbO–TeO_2 glasses crystallized with different concentrations of TiO_2 and inset represents the variation of optical band gap with concentration of TiO_2.

Table 2
Data on optical absorption spectra of ZnF_2–PbO–TeO_2:TiO_2 glass ceramic samples.

Sample	Cut-off wavelength (nm)	Band position (nm)		Optical band gap (eV)
		$^2B_{2g} \rightarrow {}^2B_{1g}$	$^2B_{2g} \rightarrow {}^2E_{1g}$	
TC_5	388	550	662	3.14
TC_7	390	558	665	3.1
TC_{10}	397	564	679	3.02
TC_{15}	396	562	677	3.05
TC_{20}	395	560	669	3.06

the intensity of this signal exhibited maximal effects at $x = 1.0$ wt%.

The infrared spectra (Fig. 7) of ZnF_2–PbO–TeO_2:TiO_2 glass ceramics exhibited the following bands [20–23]:

(i) at 460 cm^{-1} due to PbO_4 units,
(ii) 650–700 cm^{-1} due to TeO_2 axial $\nu_2(A_2) - \nu^s/TiO_6$ structural units,
(iii) 750–800 cm^{-1} due to TeO_2 equatorial $\nu_1(A_1) - \nu^s/TiO_4$ units,
(iv) 1090 cm^{-1} due to PbO_nF_m polyhedra.

As the concentration of TiO_2 is increased up to 1.0 wt%, the band due to ν^s/TiO_6 structural units is observed to grow gradually and shifts towards lower energies. A slight reversal trend in the intensity of this band could be visualized when the concentration of TiO_2 is raised beyond 1.0 wt%. The pattern of IR spectra of the amorphous samples remains the same but the variation in the relative intensity of the peaks is noticed. The comparison of these spectra with those of crystallized samples indicated that the intensity of TiO_6 band considerably lower for the pre-crystallized samples.

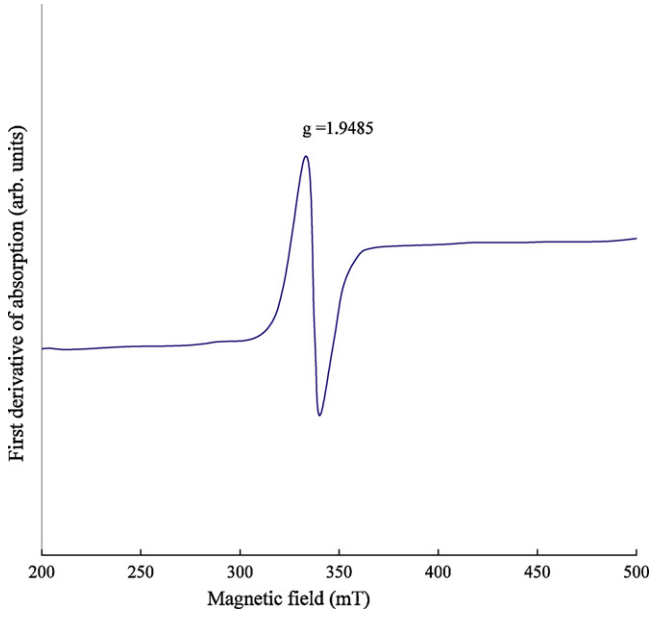

Fig. 6. ESR spectra of ZnF_2–PbO–TeO_2 glass ceramic doped with 1.0 wt% of TiO_2 recorded at room temperature.

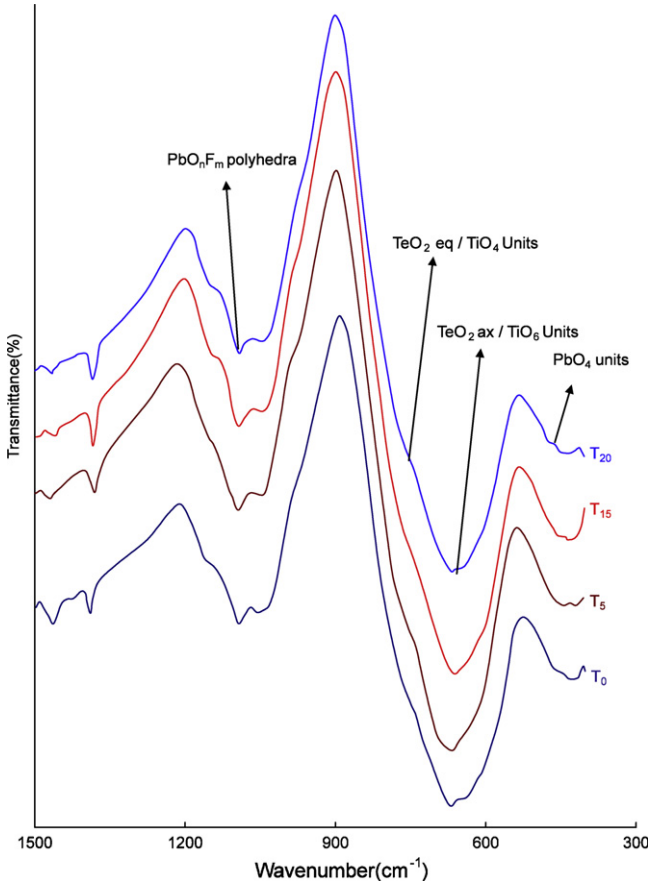

Fig. 7. IR spectra of ZnF_2–PbO–TeO_2:TiO_2 glass ceramics recorded at room temperature.

Fig. 8 represents the comparison plot of second-order susceptibility versus concentration of TiO_2 for both crystallized and pre-heated samples. The figure indicates substantial increase of the second-order optical susceptibility with the increase of TiO_2 content up to 1.0 wt%. The comparison indicates higher values of susceptibility for the crystallized samples.

Fig. 9 presents feature of electrically-induced birefringence (Δn) with the probe wavelength for the glass ceramics mixed with different concentrations of TiO_2. It is observed that the value of induced Δn is decreased with increase in probe wavelength with exhibiting a maximum at about 570 nm for the samples containing any concentration of TiO_2. It may be noted here that the birefringence for the pre-crystallized samples could not be recorded because Δn for these samples is below the detection level ($<10^{-5}$).

4. Discussion

Earlier neutron scattering experiments, IR and Raman spectral studies on TeO_2 glasses containing different modifiers have revealed that the basic building block of TeO_2 glass structure is a trigonal bipyramid commonly called TeO_4E, where one of the three equatorial directions is occupied by the $5s^2$ electronic pair (E) of the tellurium atom with two equatorial bonds [20–23]. The three-dimensional close packing is

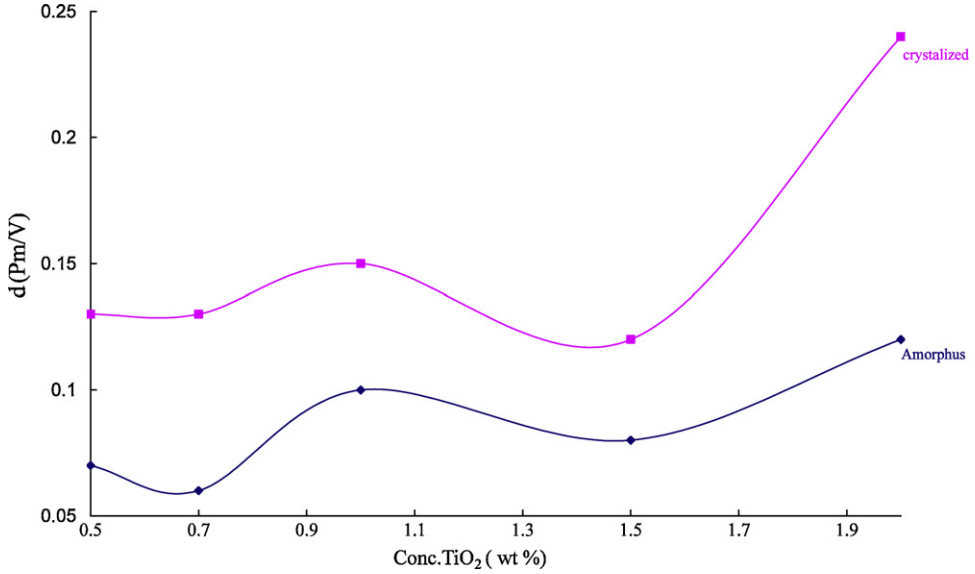

Fig. 8. Variation of second order susceptibility with the concentration of TiO_2 in ZnF_2–PbO–TeO_2 glasses and glass ceramics.

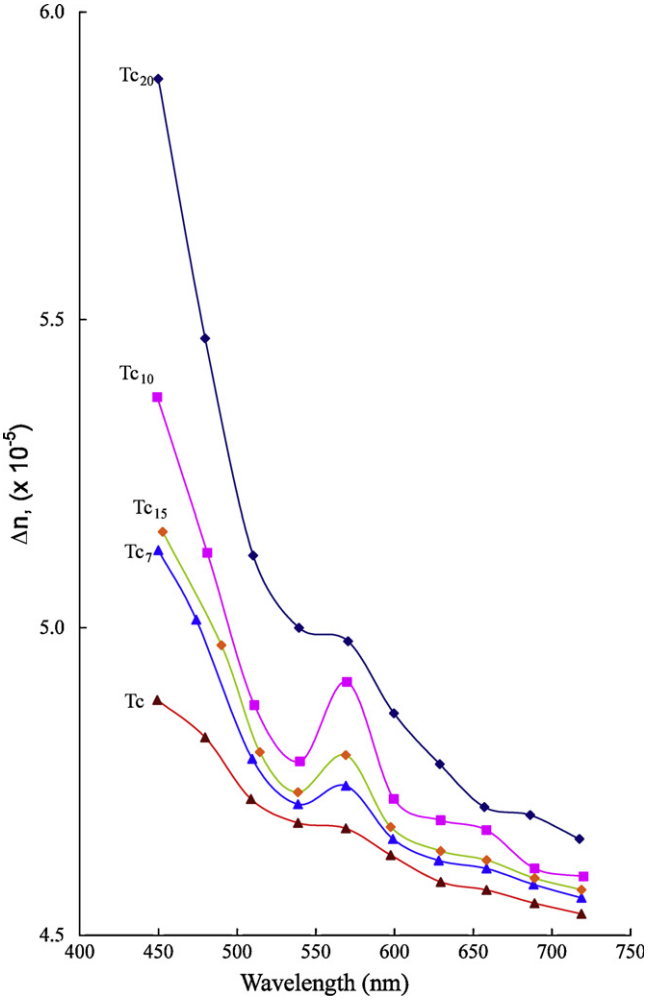

Fig. 9. Variation of change in refractive index of ZnF_2–PbO–TeO_2:TiO_2 glass ceramics with wavelength recorded at room temperature.

constituted from vertices sharing TeO_4 groups (Te_{eq}–O_{ax}–Te) reinforced by weaker Te–O interactions [24,25]. The environment of these Te atoms is completed by two other longer interactions of lengths 2.9 Å and the three dimensional close packing is constituted from vertices sharing TeO_4 groups (Te_{eq}–O_{ax}–Te) reinforced by weaker Te–O interactions of lengths 2.9 Å. In general ZnF_2 acts as modifier, fluorine ions break the Te–O bonds while Zn^{2+} ions may occupy interstitial positions or form Zn–O–Te linkages because of the close ionic radii of Te^{4+} (0.7 Å) and Zn^{2+} (0.74 Å) ions.

Titanium ions exist mainly in Ti^{4+} valence state in ZnF_2–PbO–TeO_2 glass network. Nevertheless, the reduction of Ti^{4+} to Ti^{3+} is unavoidable during melting at high temperatures and annealing processes of the glasses. Ti^{4+} ions occupy both tetrahedral and substitutional octahedral sites as corner-sharing $[TiO_6]^{2-}$ units TiO_4 units of Ti^{4+} ions enter the glass network, alternate with TeO_4 structural units and form linkages of the type Te–O–Ti, whereas, a conventional modifier oxide, Ti^{3+} ions occupy only modifying positions in the glass network.

As a modifier, Ti^{3+} ions enters the glass network by breaking up Zn–O–Te, Te–O–Te bonds and may introduce: (i) the stable $Te–O^-$ and (ii) unstable $Te–O^-$ bonds which will later be modified to $Te–O^-$ (or simply TeO_{31}) owing to the contraction of one $Te–O^-$ and the elongation of another $Te–O^-$ bond. Further, the elongation of Te–O bond of TeO_{3+1} and its cleavage finally lead to the formation of trigonal prismatic TeO_3 units (Fig. 10). Thus in addition to Te–O–Te, Zn–O–Te linkages, the structure of the titled glass network consists of TeO_4, TeO_{3+1} and TeO_3, free Zn^{2+} ions, free F^- and non bridging oxygens. Such bonding defects may increase with increase in the concentration of TiO_2.

The appearance of different crystallization temperatures in the DSC pattern obviously suggests the presence of different phases of crystallization in the samples. The crystallization in the glass samples may take place following the surface and bulk

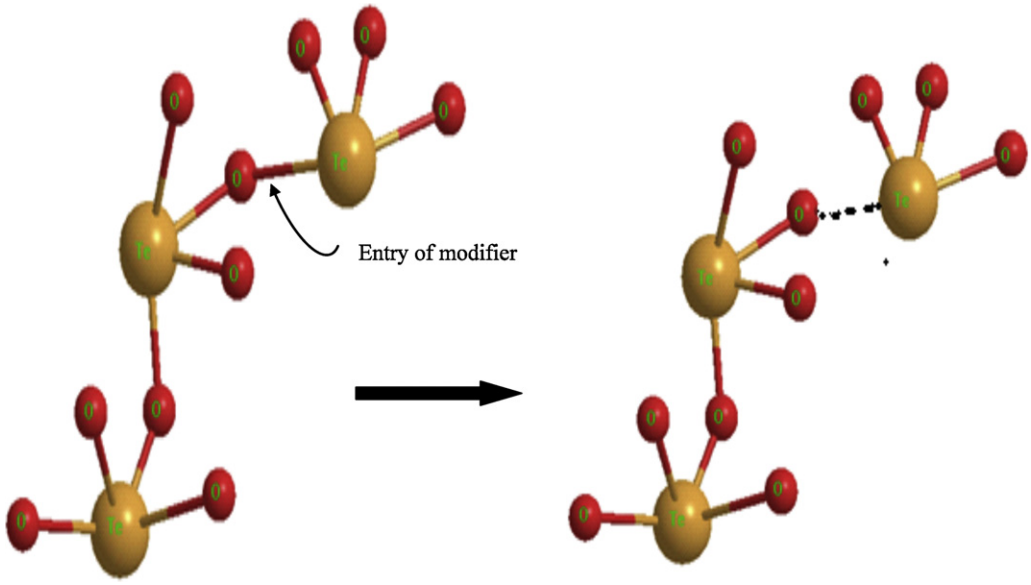

Fig. 10. An illustration for structural change in TeO_2 glass network from TeO_4 (tbp) to. TeO_{3+1} polyhedra induced by modifier. Dotted arrow indicates modifier entry.

nucleations. The general shape of the crystallization peak in DSC curves reflects the variation of enthalpy. A decrease in the value of enthalpy associated with the crystallization with increase in the nucleating agent suggests that the crystallization starts initially from the surface of the material and extended in to volume of the material. The calorimetric exothermic effects (peaks) caused by crystallization have been suppressed by mutual movement and revolution (aggregation) of metal–oxygen octahedral (endothermic) in the plastic (flexible) phase, at temperature range which appear in the same temperature as the crystallization; this effects decrease of actual enthalpy of crystallization as observed. Thermo gravimetric analysis confirms high stability and lack symptom of decomposition up to 1100 K of all the crystallized samples.

The progressive introduction of crystallizing agent TiO_2 caused a slight decrease in the density of the samples. The degree of structural compactness, the modification of the geometrical configuration of the glassy network, the size of the nano-crystals formed, change in the coordination of the glass forming ions and the fluctuations in the dimensions of the interstitial holes might have influenced the density of the glass ceramic samples.

The formation of $Pb_5Ti_3F_{19}$ crystalline phases detected from the XRD studies along with the other conventional crystalline phases emphasizes that titanium ions do exist in Ti^{3+} state in addition to Ti^{4+} state in these glass ceramics. As mentioned in the results part $Pb_5Ti_3F_{19}$ tetragonal crystalline phases exhibited three strong diffraction peaks at $2\theta = 25^\circ$, 27.84°, 29.65° reflections from (3 2 1), (4 1 1) and (2 2 2) crystal planes, respectively. The structure consists of infinite chains of eclipsed corner-sharing TiF_6 octahedra as well as individual octahedra. The arrangement and number of octahedra, PbFn polyhedra and non-octahedral F^- ions. A structural fragment of $Pb_5Ti_3F_{19}$ is illustrated in Fig. 11. Distortions from regularity in the independent TiF_6 octahedral phase result in the development of appreciable electric dipoles in these crystal phases contributing to NLO effects. The relative increase in the intensity of the diffraction peaks due to these crystallites (especially in the pattern of the samples containing TiO_2 up to 1.0 wt%) indicates larger concentration of such crystal phases. In fact ferroelectric behaviour of this type of crystals was reported earlier [26,27]. Additionally, the intensity of the diffraction peaks due to ferroelectric $PbTiO_3$, and $PbTeO_3$ phases is also found to be maximal for the samples crystallized with 1.0 wt% of TiO_2 indicating the concentration of such crystal phases is higher in this sample.

In the IR spectra, as the concentration of TiO_2 is increased up to 1.0 wt%, the band due to ν^s/TiO_6 structural units is observed to grow gradually and shifts towards lower energies. Tetragonally or substitutionally positioned octahedral Ti^{4+} ions do not induce any non-bridging oxygen ions but octahedrally positioned Ti^{3+} ions may do so [20–23] similar to Pb^{2+} ions. The highest intensity of the band due to TiO_6, structural units observed in the IR spectrum of the sample TC_{10} indicates the presence of titanium ions largely in octahedral positions and titanium ions predominantly act as modifiers.

The evidence of higher concentration Ti^{3+} ions in the sample TC_{10} can also be found from the results of optical absorption and ESR spectra. The bands observed in the optical absorption spectra at about 560 nm and 680 nm of the studied glass are assigned to $^2B_2 \rightarrow {}^2B_1$ and $^2B_2 \rightarrow {}^2E_1$ transitions of the Ti^{3+} ions, respectively [28,29]. With increase in concentration of TiO_2 up to 1.0 wt% a gradual growth of these bands could clearly be seen; this observation indicates that there is a higher fraction of Ti^{4+} ions that have been reduced in to Ti^{3+} ions. The analysis of ESR spectral results also supports this view point.

The octahedrally coordinated Ti^{3+} ions, similar to Zn^{2+} ions act as modifiers and are expected to induce non-bridging oxygens (NBO's) in the glass network. Hence there will be an increase in the degree of localization of electrons there by an enhancement of the donor centers in the glass network is possible. The presence of higher concentration of these donor

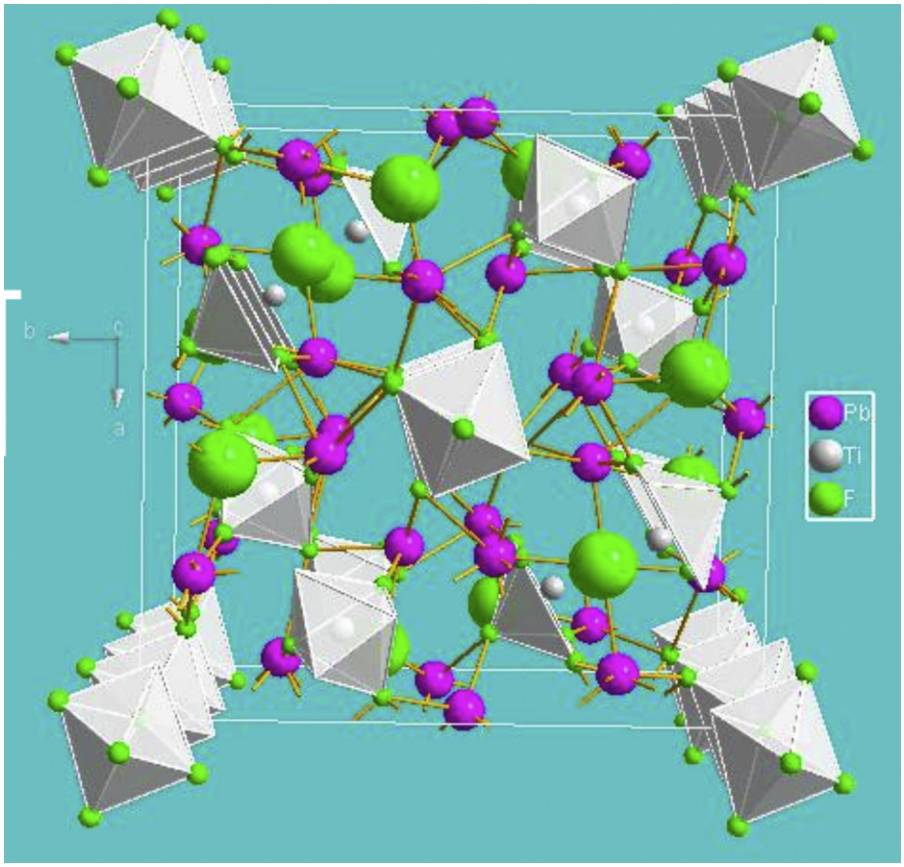

Fig. 11. An illustration of $Pb_5Ti_3F_{19}$ structural fragment.

centers decreases the optical band gap and shifts the absorption edge gradually towards higher wavelength side with increase in the concentration of TiO_2 (up to 1.0 wt%) as observed. The gradual decrease in the proportion of network forming Ti^{4+} ions in the glass network results an increase the generation of donor centers as stated above; as a consequence, there will be a increasing overlap between empty 3d states of Ti^{4+} sites and the neighbouring excited states of localized electrons originally trapped on Ti^{3+} ions. Such overlap leads to the shrinkage of optical band gap as observed (Table 2).

It is a very crucial result because the PIB maximal exists for sample TC_{10} possessing minimal optical energy gap allows to conclude that Ti ion surrounding ligands play major role in the observed NLO effects.

Under the application of high dc field, the electrical forces form orientational field which align the corresponding state dipole moments and form the macroscopic non-centrosymmetry. The coupling of this acentric field with the third order susceptibility, χ^3, gives rise to effective second-order susceptibility through the equation

$$\chi^{(2)} = 3\chi^{(3)}E_{dc} \quad (2)$$

The induced polarizability is an effective optical second order nonlinear coefficient $\chi^{(2)}$. This one is commonly believed to arise from the symmetry breaking recorded dc-electric field acting on the third-order nonlinear susceptibility as per the

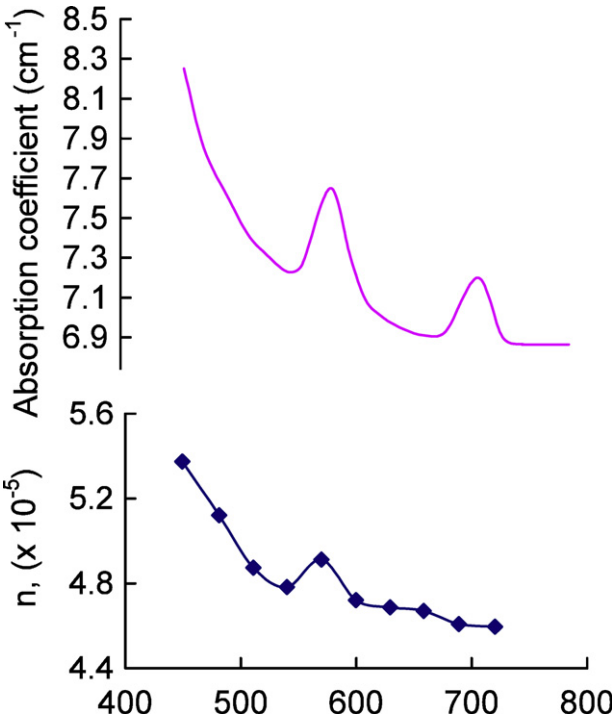

Fig. 12. A correlation graph between optical absorption and induced birefringence for the glass ceramic sample TC_{10}.

Eq. (2). In the present investigation we have observed the highest value of $\chi^{(2)}$ for the sample TC_{10}; incidentally we have observed the lowest optical band gap for the same sample. From the XRD data and even from ESR data we have observed that a major portion of titanium ions exists in Ti^{3+} state and form $Pb_5Ti_3F_{19}$ crystal phase. Such phases seemed to be facilitating for the growth of $\chi^{(2)}$ value and are responsible for higher values of $\chi^{(2)}$ for the sampleTC_{10}. However, the highest value of $\chi^{(2)}$ observed for the sample TC_{20} indicates the concentrations of conventional ferroelectric crystal phases viz., $PbTiO_3$ and also $PbTeO_3$ dominate over the $Pb_5Ti_3F_{19}$ crystal phase.

DC field-induced birefringence (Δn) with the probe wavelength of the glass ceramics (mixed with different concentrations of TiO_2) is decreased with increase in probe wavelength with exhibiting a maximum at about 570 nm ZnF_2–PbO–TeO_2 glass ceramics samples containing any concentration of TiO_2. For the sake of understanding, in Fig. 12, we have plotted combined variation of Δn and the optical absorption spectra recorded in the same wavelength region for the sample TC_{10}. The figure clearly confirms that there is a correlation between $^2B_{2g} \rightarrow {}^2B_{1g}$ transition of Ti^{3+} ion and the maximal value of Δn. This observation suggests that diffraction due to induced grating can be attributed to changes in the absorptive part (imaginary part) of the refractive index.

The relation between measured value of absorption coefficient $\Delta\alpha$ at the peak in the absorption spectrum and the changes in the real part of the refractive index $\Delta n'(\omega)$ (determined using a weak probe beam of variable frequency ω in the presence of a strong pump at the appropriate frequency) is represented by the conventional Kramers–Kronig (KK) relation as

$$\Delta n'(\omega, I) = \frac{C}{\pi} P \int_0^{\infty} \frac{\Delta\alpha(\omega', I)}{\omega'^2 - \omega^2} d\omega' \quad (3)$$

Here, P refers to Cauchy's principal value and C is the velocity of light and $\Delta\alpha = (1/LN_i)\log(I_0/I)$ with N_i being the titanium ion concentration (in mol%), L the optical path length (thickness) in cm and $\log(I_0/I)$ the optical density at the peak position. The peaking of Δn at ~570 nm in the presence of a pump, as per the Eq. (3), can therefore be attributed to the building up of maximum population by the pump at $^2B_{1g}$ level. The fall of absorption observed above this wavelength is a result of saturation.

5. Conclusions

1. ZnF_2–PbO–TeO_2 glasses doped with different concentrations of TiO_2 (0–2.0 wt%) were prepared and subsequently heated for 72 h at the temperature T_c identified from DSC studies.
2. The characterization of the samples by SEM, XRD and DSC techniques have indicated that the samples contain well defined and randomly distributed grains of different crystalline phases. The interesting tetragonal crystalline phases like $Pb_5Ti_3F_{19}$ in which the titanium ions exist as Ti^{3+} states were also detected in addition to conventional ferroelectric phases like $PbTiO_3$ and also $PbTeO_3$ samples.
3. The IR spectral studies have indicated that the glass ceramic samples contains various structural units $[TiO_6]^{2-}$, TiO_4 and TeO_4 units with the linkages of the type Te–O–Ti.
4. The analysis of the results of optical absorption, ESR spectra of the studied glass ceramics have indicated that a considerable proportion of titanium ions do exist in Ti^{3+} state in addition to Ti^{4+} state especially in the samples crystallized at about 1.0 wt% TiO_2.
5. Second order susceptibility studies (after the samples were dc field treated at elevated temperatures) with 10 ns Er: glass laser (of wavelength 1540 nm with power densities up to 1.5 GW/cm^2) and also birefringence studies have indicated that $Pb_5Ti_3F_{19}$ crystal phases do contribute to NLO effects in addition to $PbTiO_3$ and $PbTeO_3$ crystal phases.

Acknowledgement

Two of the authors V. Ravi Kumar and N. Narasimha Rao gratefully acknowledge the financial support extended by UGC, Govt. of India for carrying out this work.

References

[1] D. Ehrt, T. Kittel, M. Will, S. Nolte, A. Tunnermann, Femtosecond-laser-writing in various glasses, J. Non-Cryst. Solids 345/346 (2004) 332–337.
[2] K. Divakara Rao, K.K. Sharma, Dispersion of the induced optical non-linearity in rhodamine 6G doped boric acid glass, Opt. Commun. 119 (1995) 132–138.
[3] T. Komatsu, K. Koshiba, T. Honma, Preferential growth orientation of laser-patterned $LiNbO_3$ crystals in lithium niobium silicate glass, J. Solid State Chem. 184 (2011) 411–418.
[4] L.R. Pinckney, Transparent high strain point spinal glass-ceramics, J. Non-Cryst. Solids 255 (1999) 171–177.
[5] G.H. Beall, L.R. Pinckney, Nanophase glass-ceramics, J. Am. Ceram. Soc. (1999) 5–16.
[6] I.V. Kityk, B. Marciniak, B. Sahraoui, Photoinduced electrooptics in pyrene molecular crystallites incorporated within polymer matrices, Cryst. Res. Technol. 37 (2002) 477–484.
[7] S. Tkaczyk, M. Galceran, S. Kret, M.C. Pujol, M. Aguilo, F. Diaz, A.H. Reshak, I.V. Kityk, UV-excited piezo-optical effects in oxide nanocrystals incorporated into PMMA matrices, Acta Mater. 56 (2008) 5677.
[8] M. Williams, D. Hunter, A.K. Pradhan, I.V. Kityk, Photoinduced piezooptical effect in Er doped ZnO films, Appl. Phys. Lett. 89 (2006) 043116.
[9] R.A.H. El-Mallawany, Tellurite Glasses Handbook: Physical Properties and Data, CRC Press, Boca Raton, FL, 2002.
[10] S.H. Kim, T. Yoko, S. Sakka, Linear and nonlinear optical properties of TeO_2 glass, J. Am. Ceram. Soc. 76 (1993) 2486.
[11] N. Shimoji, T. Hashimoto, H. Nasu, K. Kamiya, Non-linear optical properties of Li_2O–TiO_2–P_2O_5 glasses, J. Non-Cryst. Solids 324 (2003) 50–57.
[12] A. Shaim, M. Et-tabirou, Role of titanium in sodium titanophosphate glasses and a model of structural units, Mater. Chem. Phys. 80 (2003) 63–67.
[13] R.K. Brow, D.R. Tallant, W.L. Warren, A. McIntyre, D.E. Day, Spectroscopic studies of the structure of titanophosphate and calcium titanophosphate glasses, Phys. Chem. Glasses 38 (1997) 300–306.
[14] P. Nageswara Rao, C. Laxmi Kanth, D. Krishna Rao, N. Veeraiah, Influence of titanium ions on optical properties of AF–PbO–B_2O_3 glasses, J. Quant. Spectrosc. Radiat. Transfer 95 (2005) 373–386.

[15] I.V. Kityk, W. Imiolek, A. Majchrowski, E. Michalski, Photoinduced second harmonic generation in partially crystallized BiB_3O_6 glass, Opt. Commun. 219 (2003) 421–426.
[16] T. Satyanarayana, I.V. Kityk, M. Piasecki, P. Bragiel, M.G. Brik, Y. Gandhi, N. Veeraiah, Structural investigations on $PbO–Sb_2O_3–B_2O_3$:CoO glass ceramics by means of spectroscopic and dielectric studies, J. Phys.: Condens. Matter 21 (2009) 245104.
[17] O.G. Vlokh, I.V. Kityk, A.V. Polovonko, Temperature dependences of optical birefringence and dielectric-constant of the $[N(CH_3)_4]_2ZnCl_4$ crystal, Ukr. Phys. J. 29 (1983) 1099–1100.
[18] Powder Diffraction File, Alphabetical Index, Inorganic Compounds, JCPDS, International Centre for Diffraction Data, Newtown Square, PA, 2003.
[19] K. Morigaki, Physics of Amorphous Semiconductors, World Scientific, Singapore, 1999, pp. 140.
[20] P. Rozier, A. Burian, G.J. Cuello, Neutron, X-ray scattering studies of $Li_2O–TeO_2–V_2O_5$ glasses, J. Non-Cryst. Solids 351 (2005) 632–639.
[21] S. Neov, I. Gerasimova, V. Kozhukharov, P. Mikula, P. Lukáš, The structure of glasses in the $TeO_2–P_2O_5$ system, Acta Phys. Hung. 75 (2009) 253–256.
[22] M.R. Sahar, K. Sulhadi, M.S. Rohani, Spectroscopic studies of $TeO_2–ZnO–Er_2O_3$ glass system, J. Mater. Sci. 42 (2007) 824–827.
[23] Y. Gandhi, N. Krishna Mohan, N. Veeraiah, Role of nickel ion coordination on spectroscopic and dielectric properties of $ZnF_2–As_2O_3–TeO_2$:NiO glass system, J. Non-Cryst. Solids 357 (2011) 1193–1202.
[24] V. Ravikumar, N. Veeraiah, Infrared spectral investigations on $ZnF_2–PbO–TeO_2$ glasses, J. Mater. Sci. Lett. 16 (1997) 1816–1818.
[25] D.K. Durga, N. Veeraiah, Role of manganese ions on the stability of $ZnF_2–P_2O_5–TeO_2$ glass system by study of dielectric dispersion and some other physical properties, J. Phys. Chem. Solids 64 (2003) 133–146.
[26] S.C. Abrahams, J. Ravez, H. Ritter, J. Ihringer, Structure–property correlation over five phases and four transitions in $Pb_5Al_3F_{19}$, Acta Crystallogr. B59 (2003) 557–574.
[27] V. Andriamampianina, P. Gravereau, J. Ravez, S.C. Abrahams, Relationship between the structures of ferroelectric $Pb_5Cr_3F_{19}$ and antiferroelectric $Pb_5Al_3F_{19}$ at 295 K and the phase III–phase IV transition in $Pb_5Al_3F_{19}$ on cooling to about 110 K, Acta Crystallogr. B50 (1994) 135–141.
[28] M.V. Ramachandra Rao, Y. Gandhi, L. Srinivasa Rao, G. Sahayabaskaran, N. Veeraiah, Electrical and spectroscopic properties of $LiF–Bi_2O_3–P_2O_5$:TiO_2 glass system, Mater. Chem. Phys. 126 (2011) 58–68.
[29] T. Satyanarayana, I.V. Kityk, K. Ozga, M. Piasecki, P. Bragiel, M.G. Brik, V. Ravikumar, A.H. Reshak, N. Veeraiah, Role of titanium valence states in optical and electronic features of $PbO–Sb_2O_3–B_2O_3$:TiO_2 glass alloys, J. Alloys Compd. 482 (2009) 283–297.